Impact of cerebellar atrophy on cortical gray matter and cerebellar peduncles as assessed by voxel-based morphometry and high angular resolution diffusion imaging

Michael Dayan, PhD[a]
Giusy Olivito, PhD[b,c]
Marco Molinari, MD, PhD[d]
Mara Cercignani, PhD[a,e]
Marco Bozzali, MD, PhD[a]
Maria Leggio, MD, PhD[b,c]

[a] Neuroimaging Laboratory, IRCCS Santa Lucia Foundation, Rome, Italy
[b] Ataxia Laboratory, IRCCS Santa Lucia Foundation, Rome, Italy
[c] Department of Psychology, Sapienza University of Rome, Rome, Italy
[d] Neurological and Spinal Cord Injury Department A, IRCCS Santa Lucia Foundation, Rome, Italy
[e] Clinical Imaging Sciences Centre, Brighton and Sussex Medical School, Falmer, UK

Correspondence to: Maria Leggio
E-mail: maria.leggio@uniroma1.it

Summary

In recent years the cerebellum has been attributed a more important role in higher-level functions than previously believed. We examined a cohort of patients suffering from cerebellar atrophy resulting in ataxia, with two main objectives: first to investigate which regions of the cerebrum were affected by the cerebellar degeneration, and second to assess whether diffusion magnetic resonance imaging (dMRI) metrics within the medial (MCP) and superior cerebellar peduncle (SCP) – namely fractional anisotropy (FA) and radial diffusivity (RD) – could be used as a biomarker in patients with this condition.
Structural and dMRI data of seven patients with cerebellar atrophy (2 with spinocerebellar atrophy type 2, 1 with Friedreich's ataxia, 4 with idiopathic cerebellar ataxia) and no visible cortical lesions or cortical atrophy were investigated with Freesurfer and voxel-based morphometry (VBM) of gray matter (GM) as well as MCP and SCP FA maps. Correlations of MCP and SCP mean FA with ataxia scores and subscores were also evaluated.
Freesurfer showed that patients had significantly reduced volume of the thalamus, ventral diencephalon and pallidum. VBM also demonstrated significantly lower local GM volumes in patients, notably in the head of the caudate nucleus, posterior cingulate gyrus and orbitofrontal cortex bilaterally, as well as in Broca's area in the left hemisphere, and a significant increase in RD in the MCP and SCP of both hemispheres. A significant correlation was found between MCP mean FA and total ataxia score (R=–0.7, p=0.03), and subscores for kinetic functions (R=–0.74, p=0.03) and oculomotor disorders (R=–0.70, p=0.04).
The regions of the cerebrum found to have significantly lower local GM volumes have been described to be involved in higher-level cerebellar functions such as initiation of voluntary movements, emotional control, memory retrieval and general cognition. Our findings corroborate recent research pointing to a more extensive corticocerebellar system than previously thought. The significant difference in the MCP and SCP dMRI metrics between patients and controls as well as the significant correlation with ataxia total score and subscores support the use of dMRI metrics as an imaging biomarker for cerebellar degeneration and ataxia.

KEY WORDS: ataxia, cerebellum, Friedreich's ataxia, magnetic resonance imaging, neurodegeneration, spinocerebellar ataxia

Introduction

The cerebellum is well known for its involvement in motor tasks. This involvement was considered, for decades, to be its main if not only significant influence on brain functions, and its study led to substantial knowledge regarding the neuroanatomical structures subserving movement coordination (Glickstein et al., 2009). Strong evidence of the active role of the cerebellum in both cognition and emotion has been progressively unveiled only in recent years, and little is known about the underlying functional/structural relationships between the cerebellum and higher-level functions (Tedesco et al., 2011; O'Halloran et al., 2012). Global cerebellar atrophy is thought to affect all regions connected to the cerebellum. For this reason, analyzing patients with this condition via whole-brain voxel-based morphometry (VBM) — this is a technique designed to investigate all aimed voxels independently — appears to be a very suitable approach for conducting exploratory research aimed at uncovering the unknown functional/structural relationships between the cerebellum and cerebrum. VBM has already been used in several cerebellar studies concerned with focal cerebellar damage (Clausi et al., 2009) as well as ataxia and cerebellar degeneration. Ataxia is the lack of coordination of voluntary movements and its most common cause is a cerebellar dysfunction of genetic origin. It generally has a progressive time course associated with cerebellar atrophy. The most frequent hereditary forms are referred to as spinocerebellar ataxia (SCA) when the pattern of inheritance is autosomal dominant, and Friedreich's ataxia in the case of an autosomal recessive origin. Despite recent advances indicating that the corticocerebellar system is more extensive than previously thought, most VBM studies on SCAs and Friedreich's ataxia demonstrated gray

matter (GM) atrophy restricted to the cerebellum, with the exception of findings of caudate nucleus involvement and of other scattered and asymmetrical regions of GM atrophy, which are nevertheless inconsistent between studies (Schulz et al., 2010; Currie et al., 2013). The first objective of this work was to use VBM in a cohort of patients with cerebellar atrophy to investigate which regions of the cerebrum were affected by the cerebellar degeneration. According to the current genetic classification there are more than 40 types of SCA (Currie et al., 2013), however a considerable overlap exists not only between the clinical symptoms of these different autosomal dominant types, but also with other hereditary forms of cerebellar atrophy such as Friedreich's ataxia, and consequently no neuroimaging techniques can distinguish between them all (Goel et al., 2011). Furthermore, no reliable biomarker has been demonstrated to inform on the state and severity of cerebellar ataxia (Currie et al., 2013), therefore a more clinically-focused aim of this study was to assess how the use of VBM and diffusion magnetic resonance imaging (dMRI) metrics may contribute to the diagnosis and treatment of patients presenting this condition. In the brain the motion of water molecules is impeded by the local microstructure, and instead of diffusing everywhere in space with equal probability the molecules tend to diffuse in a limited number of preferred directions assumed to correspond to the underlying white matter fiber bundle(s). The diffusion tensor (DT) model is a simple dMRI model which assumes only one fiber direction per voxel (more advanced methods exist to estimate multiple fiber directions). It is commonly used to quantify the diffusion process with DT-derived metrics such as fractional anisotropy (FA), mean diffusivity (MD) and radial diffusivity (RD), which relate to the tendency of water molecules to move in a particular direction (FA), in any direction (MD), and orthogonally to the underlying fiber direction (RD). FA has been shown to be positively correlated — and MD and RD negatively correlated — with fiber integrity (Beaulieu, 2002; Song et al., 2002). By interconnecting fiber directions from voxel to voxel, a process called tractography (Lazar, 2010), it is possible to reconstruct white matter (WM) tracts. The medial (MCP) and superior cerebellar peduncle (SCP) are the main WM bundles connecting the cerebellum with the cerebrum, and they act, respectively, as the main input to and output from the cerebellum. Although a few studies demonstrated that dMRI metrics were significantly different between SCA or Friedreich's ataxia patients and normal controls in the MCP and SCP, only a very few investigated the correlation between dMRI metrics within these tracts and ataxia clinical scores (Mandelli et al., 2007; Prakash et al., 2009). In this work we set out to fill this gap in the literature by investigating the relationship between dMRI metrics calculated within the MCP and SCP, reconstructed via tractography, and both total ataxia score and ataxia clinical subscores. This was done to address the second objective of this study: to better characterize the ability of dMRI metrics to act as a relevant biomarker for ataxia progression.

Methods

Ethics approval

This research project was carried out on data acquired at the Santa Lucia Foundation, Rome, Italy. It was approved by the local institutional review board and complied with the Health Insurance Portability and Accountability Act. All subjects gave written informed consent before the study initiation.

Subjects

Seven patients (4 females and 3 males; mean age±SD, 49.8±7.9 years) affected by cerebellar atrophy (ATR patients) participated in this study and were selected after visual inspection of their structural MR images to confirm that no cortical lesion or cortical atrophy was apparent. Table I provides data on the subjects' demographics and etiology. Thirty normal controls (NC subjects, 23 females and 7 males) were also recruited; they had a mean age of 54.4±5.5 years.

Clinical evaluation

During their hospitalization, the patients underwent a comprehensive neurological examination and a detailed assessment of their medical history, both performed by an expert neurologist. The presence of motor deficits was assessed quantitatively using the International Cooperative Ataxia Rating Scale (Trouillas et al., 1997) whose global score ranges from 0 (absence of any motor deficit) to 100 (highest degree of motor deficits). Patients were diagnosed with cerebellar atrophy on the basis of their clinical profile and MR imaging data. The absence of any additional brain abnormality was also investigated by inspection of MR scans. The disease duration was defined as the time from their first self-reported symptoms of ataxia. All the patients underwent

Table I - Demographic data and etiology of patients with cerebellar atrophy.

Patient	Age	Gender	Etiology	Disease duration
Patient 1	46 y	F	Friedreich's ataxia	36 y
Patient 2	51 y	M	Idiopathic cerebellar ataxia	46 y
Patient 3	42 y	F	SCA2	9 y
Patient 4	64 y	M	Idiopathic cerebellar ataxia	7 y
Patient 5	42 y	F	SCA2	3 y
Patient 6	53 y	M	Idiopathic cerebellar ataxia	22 y
Patient 7	51 y	F	Idiopathic cerebellar ataxia	12 y

SCA2=spinocerebellar atrophy type 2. Mean age ± SD was 49.8 ± 7.9 years.

gene analysis, which allowed a specific diagnosis in only three of them: two patients were diagnosed with SCA2 and one patient with Friedreich's ataxia. Four patients had ataxia of undetermined etiology (idiopathic cerebellar ataxia). The main clinical data of the studied patients are summarized in table I.

Imaging

All imaging data were obtained using a 3.0T MR scanner (Siemens Allegra, Erlangen, Germany), equipped with a circularly polarized transmit-receive coil. The maximum gradient strength was 40mT.m–1, with a maximum slew rate of 400mT.m–1.ms–1. The following sequences were collected from each studied subject: 1) dual-echo turbo spin echo (TSE), repetition time T R = 6190ms, echo time T E =12/109ms; 2) fast fluid attenuated inversion recovery (FLAIR), T R = 8170ms, T E = 96ms; 3) modified driven equilibrium Fourier transform (MDEFT) for T1 contrast (T R = 1338ms, T E = 2.4ms, matrix = 256×224×176, in-plane field of view = 250×250mm^2, slice thickness = 1mm); and 4) diffusion-weighted spin-echo echo-planar imaging (SE EPI) (TR = 7s, TE = 85ms, maximum b factor = 1000s.mm^2, isotropic resolution = 2.3mm^3).This latter sequence collects seven images with no diffusion weighting (b0) and 61 images with diffusion gradients applied in 61 non-collinear directions. Dual-echo TSE and FLAIR scans were collected for the purpose of the clinical inspection of MR scans, mentioned earlier.

T1 registration

All MDEFT volumes were first skull-stripped and registered with an affine transformation to the skull-stripped T1 ICBM152 Montreal Neurological Institute (MNI) template (2mm resolution) with FSL FLIRT (FMRIB's linear image registration tool) (Jenkinson et al., 2002). Then a non-linear registration between whole skull volumes, initialized with the previous linear registration, was performed with FSL FNIRT (FMRIB's non-linear image registration tool) (Andersson et al., 2008). The resulting transformation is subsequently referred to as "T1 to MNI".

dMRI processing and registration

dMRI volumes were corrected for eddy currents and small head movements by registering each diffusion-weighted volume to the first non-diffusion-weighted volume with a 12-parameter affine transformation using FSL (Smith et al., 2004). The brain was then segmented with the BET utility (Smith, 2002) whose parameters were adjusted after iterative visual inspection. The DT coefficients were computed with weighted linear least-square regression, as implemented in Camino (Cook et al., 2006), and then used in the calculation of the dMRI metrics, namely FA and RD. Each skull-stripped FA volume was registered to the native space skull-stripped MDEFT volume with a non-linear transformation initiated from a previous linear transform, in a manner similar to that described in the previous section (T1 registration). The resulting non-linear transform was combined with the T1 to MNI registration to register each subject's FA volume with the ICBM152 MNI template. The combined transform is referred to as "FA to MNI".

Tractography

The MCP and SCP were reconstructed according to the multi-fiber directions estimated in each voxel from the fiber orientation distribution functions (fODFs) calculated with either Q-ball imaging (Hess et al., 2006) or a statistic termed the persistent angular structure (PAS) (Jansons and Alexander, 2003). The fODF calculation method chosen depended on the curvature and amount of crossing of each WM tract. Since Q-ball, compared with PAS, tends to provide fewer false-positive fiber components while dealing less effectively with fiber crossing, it was used for the MCP reconstruction. Conversely, since the SCP is particularly difficult to reconstruct in the brain stem where it decussates, the PAS method was chosen for this tract. Once the multi-fiber directions had been estimated, probabilistic tractography was carried out based on these data using the probabilistic index of connectivity (PICo) algorithm. N = 10000 tracking iterations were performed from each voxel of the seed region of interest (ROI) applying a stopping threshold of FA ≤ 0.1 and an angle threshold of 80°. The fiber directions in every voxel were changed for each iteration according to the uncertainty associated with their estimation. Among these iterations, only tracts going through "waypoint" ROIs were selected. Alternatively, an "end-point" ROI pair was used, so as to retain only tracts where each extremity reached one of the two different end-point ROIs. Finally, tracts intersecting "exclusion" ROIs were removed and a probability map was calculated so that the PICo value of each voxel was equal to the number of remaining tracts intersecting that voxel, divided by the total number N of iterations. For the MCP, the seed was placed bilaterally in a single coronal plane, just anterior to the dentate nucleus of each cerebellar hemisphere, in regions with fibers with anterior-posterior orientation (green in color-coded FA maps). Generated tracts were made to pass through two coronal waypoint ROIs placed bilaterally, and anteriorly, to each seed ROI. Finally, an exclusion ROI was placed in an axial plane above the pons to prevent the tracts from ascending superiorly to that level, such as along the SCP. The SCP was segmented separately for each cerebellar hemisphere. For the left SCP (L-SCP), defined as originating from the left cerebellar hemisphere, the seed was placed on a single coronal slice in the dentate nucleus. We chose seed voxels whose principal direction of diffusion was not towards neighboring voxels belonging to the MCP. A pair of endpoint ROIs was drawn so that:

- the first ROI was just posterior to the seed ROI (so as to select all the fibers that continue posteriorly)
- the second ROI was placed contralaterally to include both the red nucleus and its medial area, which the SCP is known to pass through.

Two exclusion ROIs were further delineated:

- one in the whole coronal slice immediately superior to the second end-point ROI
- another in a sagittal plane so as to extend superiorly up to a few voxels below the known SCP decussation.

ROIs sagittally symmetrical to the ones just described were used for the right SCP (R-SCP).

The group-average MCP, L-SCP and R-SCP maps were calculated independently using the following procedure: first, the individual tract PICo maps were thresholded at

a value chosen to minimize the amount of volume variation depending on the PICo threshold. The curve representing the volume as a function of the PICo threshold varied; this curve took the form of a hyperbola which was fitted with the Levenberg-Marquardt algorithm. The curve vertex (i.e. its "knee") was estimated for each subject by estimating the smallest radius of curvature, after which the median among all subjects was selected as the common threshold to be applied to all PICo maps. Second, once the binarized individual maps had been obtained, the FA to MNI transformation was used on these maps to provide a group-average map in MNI space. Each voxel value in this map represented the number of subjects having this voxel as part of their tract. Finally, the subject-count threshold chosen to obtain a binary map of the "average tract" was set visually as the maximum which provided a reconstruction matching known neuroanatomy. This threshold was set to 50% for the MCP, L-SCP and R-SCP tracts.

Voxel-based morphometry

All MDEFT volumes were segmented in GM, WM and cerebrospinal fluid, and each tissue class was registered to MNI space, with an iterative combination of segmentations and normalizations as implemented by the "New Segment" and "DARTEL" routines of Statistical Parametric Mapping 8 (SPM8) (http://www.fil.ion.ucl.ac.uk/spm, Wellcome Trust Centre for Neuroimaging, Institute of Neurology University College London, UK). VBM was carried out on the modulated GM maps, to account for registration deformations, and smoothed with an 8mm full-width-at-half-maximum Gaussian kernel. NC subjects and ATR patients were entered as two independent groups while age, gender and intracranial volume (ICV) were set as nuisance variables. T-contrasts were evaluated with family-wise error (FWE) corrections at voxel level with $p<0.05$ chosen as the level of significance. Each subject FA to MNI transform was applied to their RD map which was subsequently masked with the MCP and SCP group-average binarized maps. A voxel-wise analysis comparing MCP and SCP RD between NC subjects and ATR patients was also performed on these maps in SPM8, adjusting for age and gender as explained above (with the exception that, in this analysis, ICV was not included).

Freesurfer

Differences, between ATR patients and NC subjects, in the volume of predefined GM regions were also investigated with Freesurfer (http://freesurfer.net) using its associated atlases for subcortical (Fischl et al., 2002) and cortical (Fischl et al., 2004) GM ROIs. Age, gender and ICV were accounted for when estimating volume differences, and the Bonferroni adjustment procedure was applied for multiple comparison correction.

White matter and clinical scores

The relationship between WM and clinical scores was investigated through correlations between MCP and SCP mean FA and total ataxia scores, as well as between MCP and SCP mean FA and each subtest score (posture and gait disturbances, kinetic functions, speech disorders, oculomotor disorders). Due to the limited size of our patient cohort, we increased our statistical power by assuming that a decrease in FA would result in a worse clinical score, and thus performed one-tailed Pearson product-moment correlation tests.

Results

Tractography

The MCP and SCP were successfully reconstructed in all the patients. As seen from the average tract maps in figure 1, the MCP included the transverse pontine fibers both posterior and anterior to the corticospinal tracts and the SCP featured a visible decussation at the level of the midbrain, as expected from known anatomy.

Voxel-based morphometry

Gray matter analysis

The VBM analysis demonstrated a significantly lower GM volume in the ATR patients compared with the NC subjects in a number of bilaterally symmetrical areas of the cerebellum and cerebrum. In the cerebellum, in addition to the general atrophy seen on visual inspection, the following regions demonstrated a significantly smaller local volume:

- crus I
- lobule IV
- lobule IX
- vermis VI
- vermis X

All these regions were symmetrically distributed within the cerebellum. In the cerebral cortex, the areas with a significantly lower local GM volume in the ATR patients

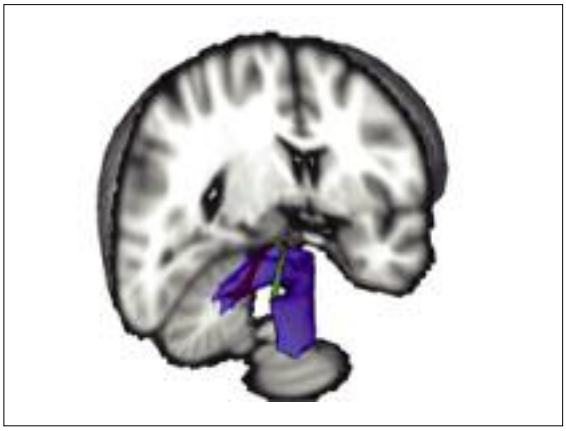

Figure 1 - Average tracts of the medial cerebellar peduncle (blue), left superior cerebellar peduncle (green) and right superior cerebellar peduncle (red) with voxels belonging to at least 50% of the subjects.
The 3D representation is viewed from a posterolateral angle. The cerebellar peduncles can be seen after removing a cube-shape volume having as its sides a sagittal plane going through the left lateral ventricle, a coronal plane just posterior to the temporal poles, and an axial plane at the level of the medulla. Note the decussation of the SCP bundles which could be reconstructed with the tractography method used.

were (Fig. 2):
- the head of the caudate nucleus
- the posterior cingulate gyrus
- the orbitofrontal cortex

Again, a marked symmetry was observed for the aforementioned areas. The only non-bilaterally symmetrical regions of significant GM differences were in the left hemisphere, Broca's area, the lingual gyrus and the secondary somatosensory cortex. The volume and MNI coordinates of the cluster peak locations are described in table II.

White matter analysis

VBM on RD maps showed that the ATR patients had significantly higher RD values than the NC subjects in both the MCP and SCP (Fig. 3). The areas of the MCP presenting these differences were located close to the pons. The SCP regions found to have significantly higher RD values, all located infratentorially, were significantly larger than the MCP regions showing significantly increased RD values.

Differences in predefined subcortical and cortical region volumes

As expected, the Freesurfer analysis demonstrated significant volume differences in the cerebellar cortex ($p<0.00005$). It also showed differences in several subcortical structures (Table III): the left and right thalamus, the left and right ventral diencephalon (which includes the hypothalamus, mammillary body, subthalamic nuclei, substantia nigra, red nucleus, medial and lateral geniculate nuclei), and the left pallidum (the right pallidum volume was no longer significantly different after Bonferonni correction). No significant differences were found in the volume of the Freesurfer cortical ROIs.

White matter and clinical score

The MCP mean FA was found to be significantly correlated with patients' total ataxia score ($R=-0.7$, $p=0.03$) (Fig. 4). On examination of the subtest scores, MCP mean FA was also found to be significantly correlated with scores for kinetic functions ($R=-0.74$, $p=0.03$) and oculomotor disorders ($R=-0.70$, $p=0.04$), while correlation of speech disorders ($R=-0.60$, $p=0.08$) and posture and gait disturbances ($R=-0.54$, $p=0.10$) scores with mean MCP FA did not reach the level of significance. No significant correlation was found between ataxia and SCP mean FA.

Discussion

Cortical and subcortical gray matter volume differences

Previous studies on the impact of cerebellar atrophy all support the occurrence of related cerebral atrophy without being conclusive, especially in seeking to determine which parts of the cerebrum were affected. Klockgether et al. (1998) investigated three types of SCA (SCA1, SCA2 and SCA3) and demonstrated smaller caudate volume for SCA3 (corresponding to the larger cohort) when compared to controls. In SCA2, Giuffrida et al. (1999) showed that in the patients studied, all suffering from cerebellar atrophy, cerebral atrophy was significant in all lobes (frontal, parietal, temporal, occipital), although the areas involved were not further specified. Only a handful of VBM studies have linked ataxia with cerebral atrophy. Brenneis et al. (2003) was the first to apply VBM to a cohort including SCA2 patients (the most common type of SCA); they found cerebral atrophy in fronto-orbital (right), temporomesial (right), frontotemporal and primary sensorimotor regions, and only in the latter two were the findings symmetrical (i.e. atrophy was found in more than one hemisphere). These results were not reproduced by Della Nave et al. (2008a) who did not find any supratentorial atrophy when examining a larger cohort of Friedriech's ataxia patients and using a more conservative VBM approach, the same as the one used in our study. Goel et al. (2011) studied SCA1, SCA2 and SCA3 patients and found atrophy in the inferior frontal, superior tem-

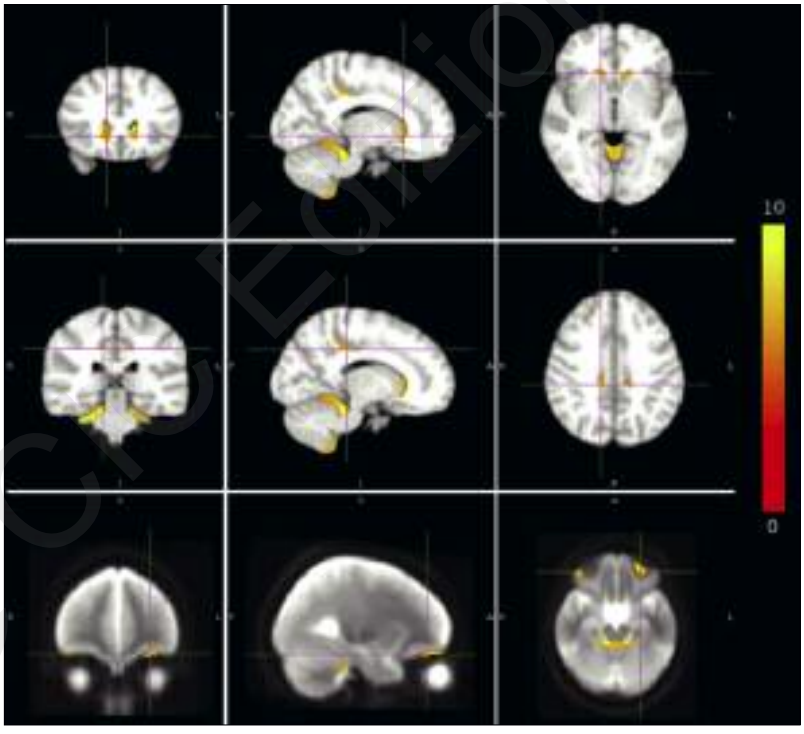

Figure 2 - Significant differences, between patients with cerebellar atrophy and normal control subjects, in gray matter local volume were found in the caudate nucleus (top), cingulate gyrus (middle) and orbitofrontal cortex (bottom).
(FWE $p<0.05$). The color bar indicates the value of the t-score, from 0 to 10.

Table II - Volume and MNI peak location of clusters with significant local gray matter volume difference as obtained from voxel-based morphometry.

Structure name	Number of voxels*	Peak MNI x (mm)	Peak MNI y (mm)	Peak MNI z (mm)
Head of caudate nucleus (left)	1412	–10.0	18.0	6.0
Head of caudate nucleus (right)	1024	14.0	23.0	–1.0
Cingulate gyrus (left)	79	–11.0	–28.0	39.0
Cingulate gyrus (medial)	120	–1.0	–27.0	27.0
Cingulate gyrus (right)	88	12.0	–31.0	40.0
Orbitofrontal cortex (left)	534	–27.0	35.0	–18.0
Orbitofrontal cortex (right)	289	37.0	33.0	–20.0
Broca's area (left)	360	–46.0	8.0	22.0
Lingual gyrus (left)	268	–20.0	–65.0	–7.0
Secondary somatosensory cortex (left)	192	–34.0	–12.0	12.0
Cerebellar cortex	23054	26.0	–33.0	–29.0

*Each voxel has a volume of 1mm^3.

Table III - Tests of cerebellar and subcortical ROI volume differences between patients with cerebellar atrophy and normal controls as obtained from Freesurfer, and corrected for age, gender and intracranial volume.

Structure name	p-value
Left accumbens	0.2980
Left amygdala	0.5170
Left caudate nucleus	0.0737
Left cerebellar cortex	< 0.00005 *
Left hippocampus	0.2012
Left pallidum	< 0.00005 *
Left putamen	0.0124
Left thalamus	0.0004 *
Left ventral diencephalon	0.0001 *
Right accumbens	0.3035
Right amygdala	0.4030
Right caudate nucleus	0.7778
Right cerebellar cortex	< 0.00005 *
Right hippocampus	0.2523
Right pallidum	0.0372
Right putamen	0.0617
Right thalamus	0.0004 *
Right ventral diencephalon	< 0.00005 *

* indicates a significant difference after Bonferroni correction.

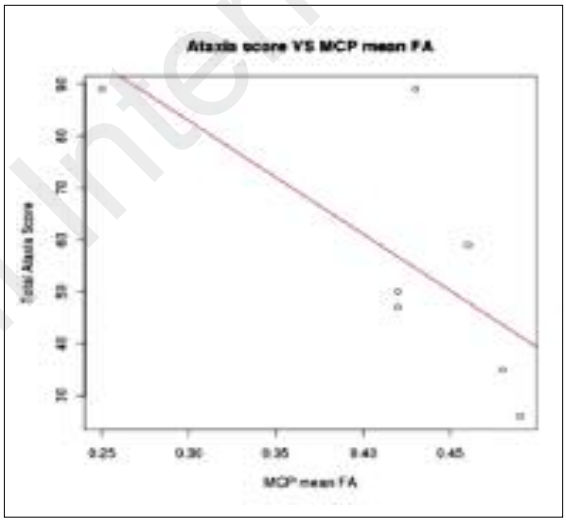

Figure 4 - Linear regression between mean fractional anisotropy of the medial cerebellar peduncle and total ataxia score.

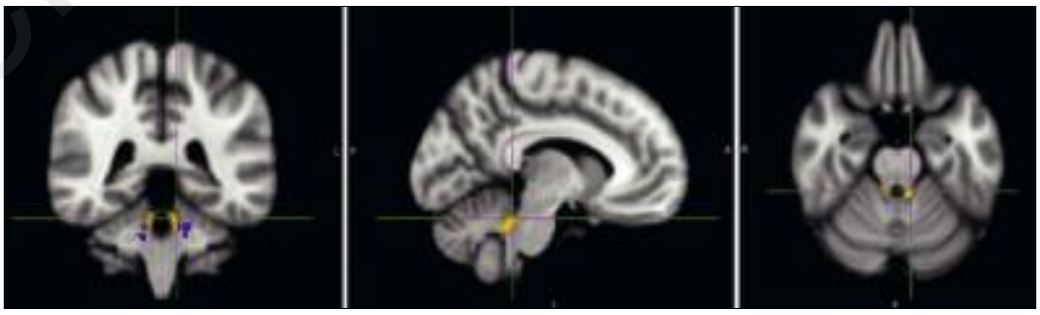

Figure 3 - Voxels with significant differences, between normal controls and patients with cerebellar atrophy, in radial diffusivity in the medial cerebellar peduncle (blue) and superior cerebellar peduncle (orange).

poral and cingulate gyri, while Schulz et al. (2010) investigated SCA1, SCA3 and SCA6 patients but the VBM statistics presented were uncorrected for multiple comparisons. The size of our patient cohort was sufficient to show significant differences with controls. In this work, we used VBM with the same conservative approach adopted by Della Nave et al. (2008a,b) and demonstrated the presence of remarkably symmetrical regions showing decreased GM local volume in patients compared with normal controls: the caudate nucleus, cingulate gyrus and orbitofrontal cortex. To the best of our knowledge, the aforementioned studies did not interpret the cortical atrophy described in their results as related to the cerebellum; conversely, this was part of the main objective of the present work. The caudate nucleus is known to be implicated, together with the cerebellum, in the initiation of voluntary movements and its head, shown in this study to have lower GM local volume in patients, has been described as receiving intensive inhibition before movement initiation. This inhibition of the caudate nucleus results in disinhibition of the cerebellar neurons and allows more effective performance of motor commands (Moroz, 2002). The posterior cingulate gyrus, shown to be involved in emotion, cognition and memory (Maddock et al., 2001, 2003) also presented a decreased GM local volume in our patients. Although we did not investigate neuropsychological scores directly, the fact that we found a change in GM volume in regions known to be involved in emotional control, memory retrieval and general cognition supports the recent idea that the cerebellum is involved in higher-level functions. Similarly, the significantly smaller GM volume in Broca's area also corroborates suggestions that the cerebellum is involved in memory retrieval and language (Silveri et al., 1998; Murdoch, 2010). Finally, as for the orbitofrontal cortex, this region has been shown in animal studies to be connected to the cerebellum through corticopontine fibers (Brodal, 1971) while in humans it has been related to cerebellar activity in various diseases and conditions (e.g. Fumal et al., 2006; Frodl et al., 2010). Differences in Freesurfer ROIs were not easily interpretable due to their relatively large size and the varied structures they encompassed, although they all included areas known to be connected with the cerebellum. Differences in ventral diencephalon volume could be due to volume differences in the red nuclei which receive many inputs from the cerebellum, while differences in thalamus volume are in line with the numerous studies on primates, which underlined the role of multiple cerebello-thalamocortical pathways for both motor and cognitive functions (Prevosto and Sommer, 2013). As regards the pallidum, the volume differences seen could be principally related to the globus pallidus, which is known to regulate the excitatory signals from the cerebellum through inhibitory processes.

Gray matter volume analysis using both voxel-based morphometry and Freesurfer

We chose to use VBM and Freesurfer analyses due to their complementary nature. On the one hand, VBM treats each voxel independently and does not make any assumption regarding the anatomy, making it possible to discover structural pattern differences that cannot be found with Freesurfer, which averages metrics over atlas regions. On the other hand, while VBM requires accurate registration and can therefore give false-positive results in the event of incorrect registration (Bookstein, 2001), Freesurfer, calculating metric averages, is more robust to misregistration. To avoid the pitfalls of VBM, each subject's registration with the SPM template was examined. From visual inspection, all the subjects were seen to be well aligned with the template. The best and worst registrations to the SPM template are shown in figure 5. This observation was further validated indirectly in our analysis by the anatomical differences, which were found to be particularly symmetrical, and located in regions known to be associated with the cerebellum. Misregistrations would most likely have created noise-like patterns, and these were not found in our results. It is to be noted that this work investigated whole-brain GM. Freesurfer studies focused on cortical GM are not restricted to volume measurements and can also investigate a variety of metrics (cortical thickness, curvature, etc.) on a high resolution mesh without requiring any atlas.

Impact of cerebellar atrophy on cerebellar peduncles

The cerebellar peduncles have been shown to be affected in SCA. In the MCP, Ginestroni et al. (2008) and Della Nave et al. (2008b), in both cases using VBM, demonstrated reduced volumes in patients (in an SCA1 and SCA2 cohort respectively), while Burk et al. (1996) showed reduced total volume in SCA1, SCA2 and SCA3 patients. Guerrini et al. (2004) and Della Nave et al. (2004) described, in SCA1 and SCA2 patients, increased MD in two small MCP ROIs (5mm diameter, one in each cerebellar hemisphere), while Ying et al. (2009) found increased MD and decreased FA in a ROI limited to a single slice in patients with olivopontocerebellar atrophy, and Mandelli et al. (2007) reported significantly higher MD and

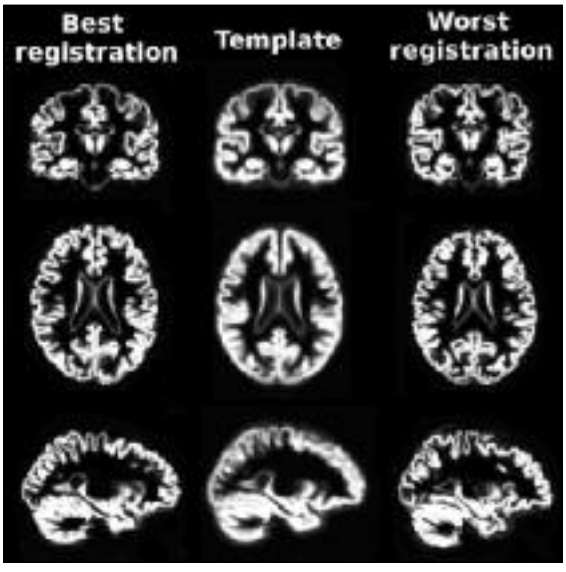

Figure 5 - Best (left) and worst (right) registration with the SPM template (middle) as selected from visual inspection. All registrations were similar but in the worst case the most superior GM regions were more flattened, most probably due to the greater atrophy of the particular subject compared to the template. Thus, the worst template registration would still detect this atrophy, but might overestimate the true degree of GM atrophy in this subject.

lower FA values in SCA1 and SCA2 patients, with statistics again restricted to small ROIs. Only a few studies reported significant differences in the SCP: Ying et al. (2009) found increased MD and decreased FA in a ROI limited to a single slice in SCA6 patients, while Mandelli et al. (2007) reported decreased FA in ROIs of a few millimeters in SCA2 patients (the difference was not found to be significant in SCA1 patients). In patients with Friedreich's ataxia, Della Nave et al. (2011) showed a significant change in all the most commonly used dMRI metrics (including FA, MD and RD) at the level of the SCP decussation (single slice) using tract-based spatial statistics, while Rizzo et al. (2011) demonstrated significantly higher MD in MCP and SCP as measured in the associated ROIs manually drawn on a single slice. The use of small ROIs can introduce important variations in the metric averaged over that region, depending on the ROI position. Reconstruction of whole WM tracts with tractography can be sensitive to ROI positioning. However, due to the characteristics of WM tracts, the average of a metric measured within a whole bundle is expected to be less sensitive to a shift in ROI position when compared to a single-slice ROI average. Tractography therefore seems to be the method of choice for the analysis of dMRI metrics within specific tracts, when the associated imaging data can be acquired, although partial volume effect in tracts as thin as the SCP are always possible. To the best of the authors' knowledge, Prakash et al. (2009) are the only ones to have used tractography for investigations in patients with SCA and/or general cerebellar atrophy; these authors applied the technique to investigate the MCP and SCP (in addition to the inferior cerebellar peduncle, ICP) and they used six diffusion gradient directions (the minimum to estimate the DT), which made it virtually impossible to resolve crossing fibers, as seen from the shape of the reconstructed SCP, which did not resemble known anatomy. This did not prevent the latter study from producing some particularly interesting results, notably significantly lower mean FA values in the MCP and SCP (as well as ICP) in SCA1 patients compared with controls. Our study is the first to use tractography with high angular resolution diffusion imaging – we used one order of magnitude more diffusion gradient directions than Prakash et al. (2009) – , and to combine it with VBM. This allowed us to localize, without any a priori hypothesis, which voxels along the tracts presented significant differences in dMRI metrics. RD was chosen over FA as it has been demonstrated to be particularly sensitive to demyelination (Alexander et al., 2007). Interestingly, we found in the MCP the same bilateral areas of significantly higher RD as in other studies investigating dMRI metrics and using the same ROIs (e.g. Guerrini et al., 2004; Della Nave et al., 2004; Mandelli et al., 2007). We also found bilaterally higher RD in a significant portion of the SCP. Unlike Della Nave et al. (2011), we did not find higher RD at the level of its decussation, however the DT model is known to fail in crossing-fiber regions in which DT metrics are thus highly unreliable.

White matter damage and clinical score

Contrary to the findings of Brenneis et al. (2003), Della Nave et al. (2004, 2008a,b), Ginestroni et al. (2008) and Ying et al. (2006), the correlation calculated in this work between cerebellar GM volume and ataxia score was not found to be significant, most probably due to the small size of our cohort. However, other studies also failed to find significant correlations with cerebellar GM volume (Prakash et al., 2009; Akhlaghi et al., 2011) and found the ataxia score to be correlated with other metrics related to the cerebellar peduncles — dMRI metrics (Prakash et al., 2009) and volume metrics (Akhlaghi et al., 2011). This suggests that total cerebellar GM volume may not be the most sensitive marker of general ataxia score and a measure of the integrity of the cerebellar peduncles may be preferable, but only a very few studies have investigated correlation between ataxia score and dMRI metrics in cerebellar peduncles. The studies of Mandelli et al. (2007) and Prakash et al. (2009) are among these; Mandelli et al. (2007) found a significant MD decrease in the MCP and an FA increase in both the MCP and the SCP to be correlated with Scale for the Assessment and Rating of Ataxia score in a cohort with SCA1 and cerebellar atrophy, while Prakash et al. (2009) described an association of FA and Neurological Exam-Based Ataxia Score in all peduncles without indicating whether these associations were significant. To the best of our knowledge, our study is the first to show a significant correlation of MCP FA with both ataxia total score and some of its subscores (kinetic functions and oculomotor disorders). These results support the use of dMRI metrics in clinical settings as a useful marker of symptomatic dysfunctions in patients presenting cerebellar atrophy. It is important to underline that no correction was performed to account for the multiple correlations calculated. The Bonferroni correction would have been too conservative as the ataxia score and its subscores are not independent observations; that said, since no correction was utilized, our results require further validation, ideally in a bigger cohort. In conclusion, by comparing patients presenting general cerebellar atrophy with normal controls, we were able to investigate which cerebral regions were affected by their cerebellar atrophy. Our analysis suggests involvement of the head of the caudate nucleus, Broca's area, and the orbitofrontal and posterior cingulate gyri in the corticocerebellar system. These results are in line with recent research which suggests that these areas are associated with higher-level cerebellar functions, namely initiation of voluntary movements, emotional control, memory retrieval and general cognition. Furthermore, the regions found to be affected were remarkably symmetrical, despite our using VBM, a statistical method that treats each voxel independently, and this lends further neuroanatomical support to our results. More generally, the cerebral regions found to be associated with cerebellar atrophy corroborate the description of the cerebellum as an important component of the brain's higher-level functions. By using, for the first time, MCP and SCP tractography in conjunction with VBM in a cohort of patients with ataxia, we were able to pinpoint locations within these tracts where dMRI metrics were significantly different from the findings in normal controls. Adding to the significant correlation found between dMRI metrics and ataxia total score and some of its subscores, these results suggest that dMRI metrics could serve as an important imaging biomarker for the diagnosis and treatment evaluation of patients suffering from ataxia. In the present study no attempt was made to differentiate between different kinds of ataxia and the findings presented may encourage further studies addressing MCP and SCP characteristics in different types of ataxia.

References

Akhlaghi H, Corben L, Georgiou-Karistianis N, et al (2011). Superior cerebellar peduncle atrophy in Friedreich's ataxia correlates with disease symptoms. Cerebellum 10:81-87.

Alexander AL, Lee JE, Lazar M, et al (2007). Diffusion tensor imaging of the brain. Neurotherapeutics 4:316-329.

Andersson J, Smith S, Jenkinson M (2008). FNIRT-FMRIB's non-linear image registration tool, In: 14th Annual Meeting of the Organization for Human Brain Mapping (OHBM), Melbourne, Australia, pp. 15-19.

Beaulieu C (2002). The basis of anisotropic water diffusion in the nervous system - a technical review. NMR Biomed 15: 435-455.

Bookstein FL (2001). "Voxel-based morphometry" should not be used with imperfectly registered images. Neuroimage 14:1454-1462.

Brenneis C, Bösch SM, Schocke M, et al (2003). Atrophy pattern in SCA2 determined by voxel-based morphometry. Neuroreport 14:1799-1802.

Brodal P (1971). The corticopontine projection in the cat. II. The projection from the orbital gyrus. J Comp Neurol 142: 141-151.

Bürk K, Abele M, Fetter M, et al (1996). Autosomal dominant cerebellar ataxia type I clinical features and MRI in families with SCA1, SCA2 and SCA3. Brain 119:1497-1505.

Clausi S, Bozzali M, Leggio MG, et al (2009). Quantification of gray matter changes in the cerebral cortex after isolated cerebellar damage: a voxel-based morphometry study. Neuroscience 162:827-835.

Cook PA, Bai Y, Gilani NS, et al (2006). Camino: Open-source diffusion-MRI reconstruction and processing, In: 14th Scientific Meeting of the International Society for Magnetic Resonance in Medicine, Seattle, USA, pp. 2759.

Currie S, Hadjivassiliou M, Craven IJ, et al (2013). Magnetic resonance imaging biomarkers in patients with progressive ataxia: current status and future direction. Cerebellum 12:245-266.

Della Nave R, Ginestroni A, Diciotti S, et al (2011). Axial diffusivity is increased in the degenerating superior cerebellar peduncles of Friedreich's ataxia. Neuroradiology 53:367-372.

Della Nave R, Ginestroni A, Giannelli M, et al (2008a). Brain structural damage in Friedreich's ataxia. J Neurol Neurosurg Psychiatry 79:82-85.

Della Nave R, Ginestroni A, Tessa C, et al (2008b). Brain white matter damage in SCA1 and SCA2. An in vivo study using voxel-based morphometry, histogram analysis of mean diffusivity and tract-based spatial statistics. Neuroimage 43:10-19.

Della Nave R, Foresti S, Tessa C, et al (2004). ADC mapping of neurodegeneration in the brainstem and cerebellum of patients with progressive ataxias. Neuroimage 22:698-705.

Fischl B, van der KouweA, Destrieux C, et al (2004). Automatically parcellating the human cerebral cortex. Cereb Cortex 14:11-22.

Fischl B, Salat DH, Busa E, et al (2002). Whole brain segmentation: automated labeling of neuroanatomical structures in the human brain. Neuron 33:341-355.

Frodl T, Bokde AL, Scheuerecker J, et al (2010). Functional connectivity bias of the orbitofrontal cortex in drug-free patients with major depression. Biol Psychiatry 67:161-167.

Fumal A, Laureys S, Di Clemente L, et al (2006). Orbitofrontal cortex involvement in chronic analgesic-overuse headache evolving from episodic migraine. Brain 129:543-550.

Ginestroni A, Della Nave R, Tessa C, et al (2008). Brain structural damage in spinocerebellar ataxia type 1: a VBM study. J Neurol 255:1153-1158.

Giuffrida S, Saponara R, Restivo DA, et al (1999). Supratentorial atrophy in spinocerebellar ataxia type 2: MRI study of 20 patients. J Neurol 246:383-388.

Glickstein M, Strata P, Voogd J (2009). Cerebellum: history. Neuroscience 162:549-559.

Goel G, Pal PK, Ravishankar S, et al (2011). Gray matter volume deficits in spinocerebellar ataxia: an optimized voxel based morphometric study. Parkinsonism Relat Disord 17:521-527.

Guerrini L, Lolli F, Ginestroni A, et al (2004). Brainstem neurodegeneration correlates with clinical dysfunction in SCA1 but not in SCA2. A quantitative volumetric, diffusion and proton spectroscopy MR study. Brain 127:1785-1795.

Hess CP, Mukherjee P, Han ET, et al (2006). Q-ball reconstruction of multimodal fiber orientations using the spherical harmonic basis. Magn Reson Med 56:104-117.

Jansons KM, Alexander DC (2003). Persistent angular structure: new insights from diffusion magnetic resonance imaging data. Inverse Problems19:1031-1046.

Jenkinson M, Bannister P, Brady M, et al (2002). Improved optimization for the robust and accurate linear registration and motion correction of brain images. Neuroimage 17:825-841.

Klockgether T, Skalej M, Wedekind D, et al (1998). Autosomal dominant cerebellar ataxia type I. MRI-based volumetry of posterior fossa structures and basal ganglia in spinocerebellar ataxia types 1, 2 and 3. Brain 121:1687-1693.

Lazar M (2010). Mapping brain anatomical connectivity using white matter tractography. NMR Biomed 23:821-835.

Maddock RJ, Garrett AS, Buonocore MH (2003). Posterior cingulate cortex activation by emotional words: fMRI evidence from a valence decision task. Hum Brain Mapp 18:30-41.

Maddock RJ, Garrett AS, Buonocore MH (2001). Remembering familiar people: the posterior cingulate cortex and autobiographical memory retrieval. Neuroscience 104:667-676.

Mandelli ML, De Simone T, Minati L, et al (2007). Diffusion tensor imaging of spinocerebellar ataxias types 1 and 2. AJNR Am J Neuroradiol 28:1996-2000.

Moroz V (2002). Roles of the caudate nuclei, cerebellum, and caudato-cerebellar interconnections in the control and coordination of ballistic food-procuring movements. Neurophysiology 34:395-405.

Murdoch BE (2010). The cerebellum and language: historical perspective and review. Cortex 46:858-868.

O'Halloran CJ, Kinsella GJ, Storey E (2012). The cerebellum and neuropsychological functioning: a critical review. J Clin Exp Neuropsychol 34:35-56.

Prakash N, Hageman N, Hua X, et al (2009). Patterns of fractional anisotropy changes in white matter of cerebellar peduncles distinguish spinocerebellar ataxia-1 from multiple system atrophy and other ataxia syndromes. Neuroimage 47 Suppl 2:T72-81.

Prevosto V, Sommer MA (2013). Cognitive control of movement via the cerebellar-recipient thalamus. Front Syst Neurosci 7:56.

Rizzo G, Tonon C, Valentino ML, et al (2011). Brain diffusion-weighted imaging in Friedreich's ataxia. Mov Disord 26: 705-712.

Schulz JB, Borkert J, Wolf S, et al (2010). Visualization, quantification and correlation of brain atrophy with clinical symptoms in spinocerebellar ataxia types 1, 3 and 6. Neuroimage 49:158-168.

Silveri MC, Di Betta AM, Filippini V, et al (1998). Verbal short-term store-rehearsal system and the cerebellum. Evidence from a patient with a right cerebellar lesion. Brain 121:2175-2187.

Smith SM, Jenkinson M, Woolrich MW, et al (2004). Advances in functional and structural MR image analysis and implementation as FSL. Neuroimage 23, Suppl 1:S208-219.

Smith SM (2002). Fast robust automated brain extraction. Hum Brain Mapp 17:143-155.

Song SK, Sun SW, Ramsbottom MJ, et al (2002). Dysmyelination revealed through MRI as increased radial (but unchanged axial) diffusion of water. Neuroimage 17:1429-1436.

Tedesco AM, Chiricozzi FR, Clausi S, et al (2011). The cerebellar cognitive profile. Brain 134:3672-3686.

Trouillas P, Takayanagi T, Hallett M, et al (1997). International Cooperative Ataxia Rating Scale for pharmacological assessment of the cerebellar syndrome. J Neurol Sci145: 205-211.

Ying SH, Landman BA, Chowdhury S, et al (2009). Orthogonal diffusion-weighted MRI measures distinguish region-specific degeneration in cerebellar ataxia subtypes. J Neurol 256: 1939-1942.

Ying SH, Choi SI, Perlman SL, et al (2006). Pontine and cerebellar atrophy correlate with clinical disability in SCA2. Neurology 66:424-426.